Available online at www.sciencedirect.com
SCIENCE DIRECT®
ELSEVIER
Applied Surface Science 218 (2003) 281–289
applied surface science
www.elsevier.com/locate/apsusc

Characterization of tungsten oxide films produced by reactive pulsed laser deposition

G. Soto*, W. De La Cruz, J.A. Díaz, R. Machorro, F.F. Castillón, M.H. Farías

Centro de Ciencias de la Materia Condensada, UNAM, Apdo. Postal 2681, 22800 Ensenada B.C., Mexico

Received 3 March 2003; accepted 18 April 2003

Abstract

Tungsten oxide thin films have been prepared by reactive pulsed laser deposition (PLD). Substrate heat treatment and oxygen partial pressure during growth are correlated with Auger electron (AES), X-ray photoelectron (XPS), electron energy loss (EELS) and transmittance spectroscopies. Electronic and mass densities, composition and chemical states are strongly dependent of the deposition conditions. No significant change in the oxygen content in films as a function of substrate or annealing temperature is detected. However, the colored state turns out to be associated to the degree of chemical disorder in the samples, as evidenced by the peak shape of the W 4f transition. Also, the strength of a characteristic energy loss at 6–7 eV appears to be related to the presence of the colored state.

Keywords: Tungsten oxide; Pulsed laser deposition; Optical properties; XPS; AES; EELS; Deposition conditions; Characterization methods

1. Introduction

Tungsten oxide is perhaps the most studied material on regards to its chromogenic properties. The singular feature of these materials is the capability of being commuted reversibly between two different optical states [1,2]. This property is valuable, for example in 'smart window', electro-optical components and displaying applications, and has been studied to a large extent with that purpose. Even with the large amount of work on different coloration effects of tungsten oxide films, many incompatible results are still reported and the elucidation of data is still under dispute [3]. A recent review in the topic by Bange [4] points out the reason of this dilemma to be that the results are compared from experiments out on, in principle, 'different' materials, even if all the films are named WO_3. His arguments are that the various deposition techniques used to produce the films on different substrates are creating very different properties and, in general, the as-deposited state, which is the base of the chromogenic behavior, is different in terms of density, composition and structure.

Independently that these arguments might be correct; the dispute will need to be clarified by thorough characterization. However, very little work is available with in situ spectroscopic characterization of the as-deposited tungsten oxide. In this work, the issue of WO_3 films growth by pulsed laser deposition (PLD) and its spectroscopic characterization is explored. The

* Corresponding author. Present address: CCMC, UNAM, P.O. Box 439036, San Ysidro, CA 92143-9036, USA. Tel.: +52-646-1744602; fax: +52-646-1744603.
E-mail address: gerardo@ccmc.unam.mx (G. Soto).

0169-4332/$ – see front matter
doi:10.1016/S0169-4332(03)00677-9

purpose is to correlate the effects of the preparation conditions, like heating of substrates and oxygen environments, in the composition, chemical and coloration states. Although we conclude that PLD might not be an ideal technique to process WO_3, these results can be of help to understand the properties of WO_3 films deposited by other techniques.

2. Experimental

2.1. Films preparation

All films were deposited in a modified laser ablation system, Riber LDM-32, with in situ Auger electron (AES), X-ray photoelectron (XPS), electron energy loss (EELS) spectroscopies. Films were deposited on two different substrates: Corning glass slides and as-received (1 1 1) *n*-doped silicon wafers. The substrate temperature was held at room temperature (RT), 250 or 500 °C for the duration of depositions. The sample identification code is P_XT_Y, where P_X denotes the oxygen pressure, P_O (in mTorr, 1 mTorr = 0.13 Pa), and T_Y denotes the substrate temperature, T_S (in °C), see Table 1. The deposition was accomplished by ablating a tungsten target (99.9 wt.%) in a background of high-purity molecular oxygen in the 1×10^{-8} to 0.1 Torr pressure range. Target ablation was accomplished by means of a KrF excimer laser ($\lambda = 248$ nm) focused on a target at 50 ° off the surface normal. Laser energy, deposition time and pulse repetition rate were fixed at 250 mJ, 10 min and 40 Hz, respectively, for a total of 24,000 laser pulses for each film except samples $P_{75}T_{RT}$ and $P_{100}T_{RT}$ deposited on silicon, which were grown for 2 min and 4800 laser pulses.

2.2. Films characterization

Electron spectroscopic analyses were performed after completion of deposition in an adjacent analysis chamber. This chamber is equipped with an electron energy analyzer Mac-3, from Cameca, suitable for AES, EELS and XPS. For the AES measurements, the incident electron beam energy was set to 3000 eV and the data acquisition was performed at a nominal resolution of 1.5 eV. EELS data were collected using an incident e-beam of 1200 eV and a resolution of 2 eV, measured from the full-width at half-maximum (FWHM) of backscattered electrons. XPS data were collected after exciting the sample by an unmonochromatized Al Kα line (at 1486.6 eV). The energy scale was calibrated against the Cu $2p_{3/2}$ and Ag $3d_{5/2}$ references, at 932.67 and 368.26 eV, respectively. The substrate signal, Si 2p at 100.0 eV, was used as reference to compensate for charge-induced energy shifting in the films. Damage on the samples, like reduction, induced by electron beam or X-ray radiation was reduced by defocusing the electron beam of AES and EELS measurements and by reducing the thickness of the deposited films, particularly for the high oxygen pressure depositing conditions. With

Table 1
Summary of tungsten oxide films prepared on glass substrates[a]

Samples	P_O (mTorr)	T_S (°C)	C_W (at.%)	C_O (at.%)	Coloration (to the naked eye)
P_0T_{RT}	Base pressure	RT	90.0 ± 3.1	10.0 ± 3.1	Metallic
P_5T_{RT}	5	RT	41.4 ± 2.0	58.6 ± 2.0	Metallic
$P_{25}T_{RT}$	25	RT	28.5 ± 1.6	71.5 ± 1.6	Metallic with a brown shine
$P_{50}T_{RT}$	50	RT	25.5 ± 1.6	74.5 ± 1.6	Blue
$P_{50}T_{250}$	50	250	27.1 ± 1.4	72.9 ± 1.4	Blue
$P_{50}T_{500}$	50	600	26.9 ± 1.3	73.1 ± 1.3	Dark blue
$P_{75}T_{RT}$	75	RT	25.9 ± 1.7	74.1 ± 1.7	Very light blue
$P_{75}T_{250}$	75	250	24.7 ± 1.2	75.3 ± 1.2	Light blue
$P_{75}T_{500}$	75	500	25.8 ± 1.3	74.2 ± 1.3	Blue
$P_{100}T_{RT}$	100	RT	26.0 ± 1.5	74.0 ± 1.5	Transparent
$P_{100}T_{250}$	100	250	25.0 ± 1.6	75.0 ± 1.6	Transparent with a pale blue shine
$P_{100}T_{500}$	100	500	25.4 ± 1.6	74.6 ± 1.6	Very light blue

[a] The C_W and C_O columns correspond to the atomic concentration as determined by XPS.

the above-mentioned experimental conditions, no considerable modification of the relative peak intensities was detected during measurements.

The studies of film optical properties were completed ex situ by transmittance spectroscopy in a Perkin-Elmer 330 spectrophotometer. In order to verify the chromogenic properties of the processed films, a selected set (films with deep-blue coloration) were thermally treated to switch their optical states. For bleaching the films, they were exposed to air in a tubular furnace at 300 °C for 4 h and for coloring, in an ultra-high vacuum (UHV) heater at 500 °C for 24 h. After thermal treatment, films were characterized again by using the available electronic spectroscopies.

2.3. Data analysis

In this work, the elemental quantification was performed by using a recently proposed scheme based on XPS measurements [5]. First, it is assumed the film matrix to be homogeneous WO_x. Then, the XPS intensity for a core level k can be written as

$$I_k \propto I_0 n \sigma_k \lambda_{MED}(E_k) T(E_k) \quad (1)$$

where n is the atomic density of the film, σ_k the photoionization cross-section for the level k [6], $\lambda_{MED}(E_k)$ the mean escape depth for electrons with kinetic energy E_k in the examined material [7] and $T(E_k)$ is the spectrometer transmission function [8]. I_0 is a constant factor, which depends on the X-ray radiation intensity. The product $\sigma_k \lambda_{MED}(E_k) T(E_k)$ is designated as the relative sensitivity factor, S_r, for the core level k. All these factors were calculated for W $4f_{7/2}$ and O 1s transitions in tungsten oxide using the electron analyzer Cameca Mac-3 transmission function and an Al Kα X-ray source. This method gives better accuracy to calculate the elemental concentrations than the traditional routine using "standard" XPS sensitivity factors from pure elements.

The electronic (ρ_e) and mass (ρ_m) densities were calculated by the collective bulk-plasmon energy, E_p, determined from the EELS measurements. Equations linking E_p to ρ_e and ρ_m can be derived from the free-electron approximation and are given by

$$\rho_e = \frac{m_e \varepsilon_0}{\hbar^2 e^2} E_p^2 = (7.2522 \times 10^{20}\,\mathrm{eV^{-2}\,cm^{-3}}) E_p^2 \quad (2)$$

$$\rho_m = \frac{m_e \varepsilon_0 E_p^2 \sum_{k=1}^{n} M_k F_k}{\hbar^2 e^2 N_A \sum_{k=1}^{n} C_k F_k} = 1.204 \times 10^{-3}\,\mathrm{eV^{-2}\,cm^{-3}} \frac{E_p^2 \sum_{k=1}^{n} M_k F_k}{\sum_{k=1}^{n} C_k F_k} \quad (3)$$

where m_e is the electron mass, e the electron charge, ε_0 the permittivity of free space, N_A the Avogadro number and $\hbar$ is the Planck's constant divided by 2π; C_k is the number of electrons contributed by the atom k (six for W and six for O) and M_k and F_k are the mass and the relative atomic fraction of the atom k (determined by XPS).

3. Results and discussion

3.1. Variation of deposition parameters

The important parameters adjusted in this work are the oxygen pressure, P_O, and substrate temperature, T_S. The sample identification label, preparation conditions, perceived coloration and the atomic concentrations for all films prepared on glass slide substrates are summarized in Table 1. For $P_O \leq 25$ mTorr, film characteristics are metallic, i.e. opaque and conductive. However, for $50 \leq P_O \leq 75$ mTorr, we obtain blue colored films, becoming transparent for $P_O = 100$ mTorr. Consequently, the obtained coloration is clearly dependent on P_O. Likewise, there is some dependency on the depth of coloration as a function of T_S. However, this effect is subtle for samples prepared at $P_O = 100$ mTorr and hardly detected by naked eye for the $P_{100}T_{RT}$, $P_{100}T_{250}$ and $P_{100}T_{500}$ samples.

3.2. Quantitative analysis

The obtained XPS and AES spectra indicate all the prepared films to contain only tungsten and oxygen, as it is shown in Fig. 1 for the Auger spectrum of a film prepared at $P_O = 75$ mTorr and $T_S = RT$. In Table 1, it can be seen that even for films prepared in ultra-high vacuum conditions there is some oxygen present, about 10 at.%. We believe this oxygen to be originated from the utilized tungsten target since XPS and Auger spectra, carried out immediately after laser ablating the tungsten target surface in UHV conditions, show some amount of oxygen on its surface.

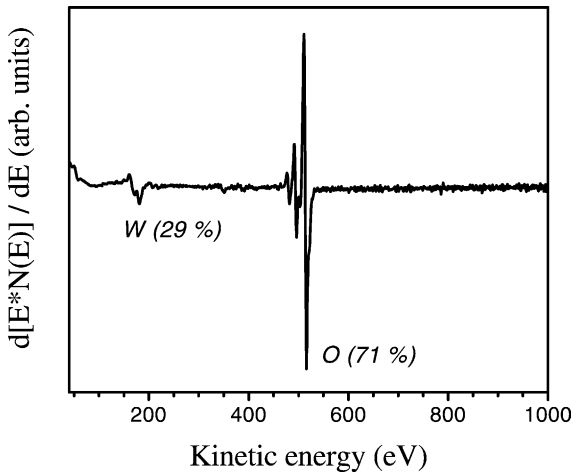

Fig. 1. AES spectrum for a film prepared at $P_O = 75$ mTorr and $T_S =$ RT. By using standard sensitivity factors the chemical composition matches, roughly, WO_3.

Fig. 2 shows the W and O atomic concentration as a function of P_O as obtained by means of XPS. As expected, the tungsten–oxygen reaction is very effective and for a relatively low P_O value of 25 mTorr, the oxygen concentration almost reaches saturation. After that deposition pressure (for $P_O = 50$, 75 and 100 mTorr), the O atomic concentration, C_O, to W atomic concentration, C_W (C_O/C_W ratio), remains about constant within the experimental uncertainty. In the saturation regime, the stoichiometric formula,

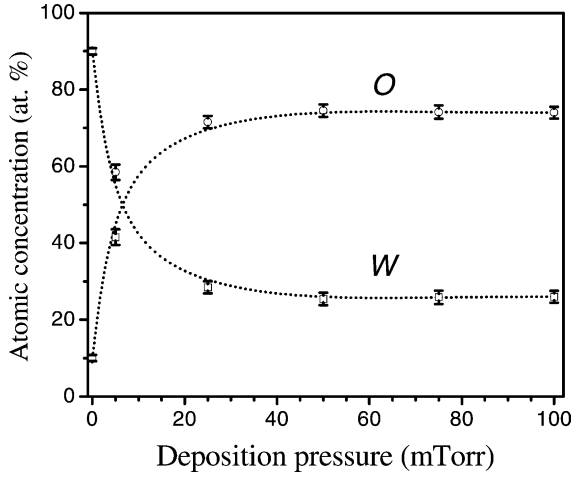

Fig. 2. W (squares) and O (circles) atomic concentrations determined by high-resolution XPS as a function of oxygen deposition pressure.

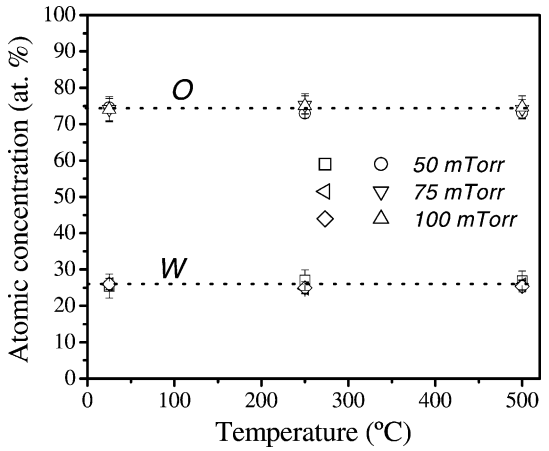

Fig. 3. W and O atomic concentrations determined by high-resolution XPS as a function of deposition temperature.

deduced from the above-mentioned calculation, corresponds to $WO_{3\pm0.3}$. Fig. 3 shows the W and O atomic concentration as a function of T_S for those pressures. From this graph, it is evident that the C_O/C_W ratio remains about constant, indicating that T_S does not induce notorious changes in the stoichiometric ratios.

On the other hand, by considering the AES measurements on all samples and performing the quantification using standard sensitivity factors [9], a small under-estimation of the oxygen concentration and a corresponding over-estimation of tungsten, of about 4–5 at.%, appears when comparing with the XPS calculations.

Consequently, as of our quantitative analysis, we conclude that for films prepared between $50 \leq P_O \leq 100$ mTor, and RT $\leq T_S \leq 500$ °C, the stoichiometric concentrations are constant and fall within our experimental uncertainty, which is about ±1.8 at.% obtained from the standard deviation of data in Fig. 3.

3.3. Chemical states

The chemical states of the W and O atoms in the WO_x films were determined by means of XPS. The shifts of the core-electron binding energy are the result of charge transfer between W and O atoms. Then, the high difference of electronegativity between the two involved atoms is assumed to result in two different spectroscopic characteristics, as it was already appreciated by Shen and Mai [10]. Thereafter, the oxide and

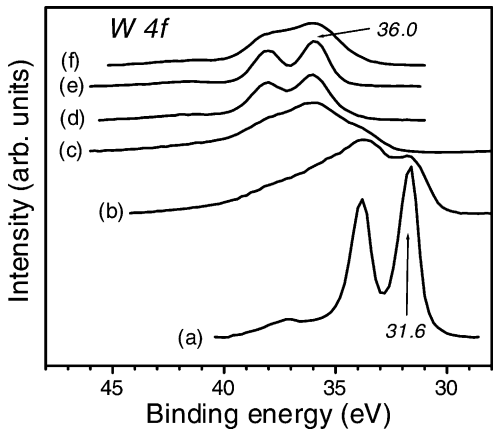

Fig. 4. W 4f transition and its chemical shift as a function of oxygen pressure during film deposition for samples: (a) P_0T_{RT}, (b) P_5T_{RT}, (c) $P_{25}T_{RT}$, (d) $P_{50}T_{RT}$, (e) $P_{75}T_{RT}$ and (f) $P_{100}T_{RT}$. Curves have been vertically offset and the peak-areas normalized according to their relative atomic concentrations.

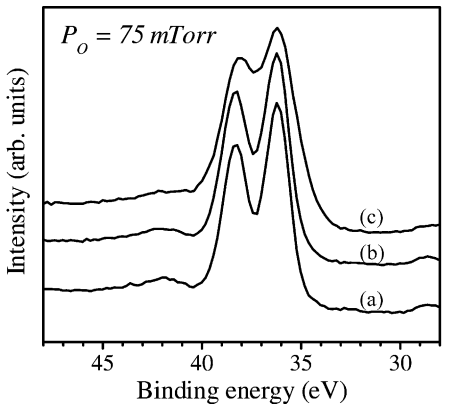

Fig. 5. W 4f transition for different substrate temperatures of samples: (a) $P_{75}T_{RT}$, (b) $P_{75}T_{250}$ and (c) $P_{75}T_{500}$. For clarity, curves have been vertically offset.

the metallic counterpart should be clearly distinguishable between them in XPS. Fig. 4 shows the high-resolution W 4f transition, acquired on films prepared in the $0 \leq P_O \leq 100$ mTorr pressure range and deposited on silicon substrates. For clarity, in this graph the intensities have been offset vertically and the peak-areas normalized according to their relative atomic concentrations. As expected, a shift in the peak positioning occurs while oxygen is incorporated in the material; from 31.6 eV on the W $4f_{7/2}$ transition for the P_0T_{RT} sample, up to 36.0 eV for the $P_{75}T_{RT}$ sample, in good agreement with the reported energy for WO_3 [11–13]. The films prepared at 5 and 25 mTorr, lines b and c of Fig. 4, show an undefined superposition of different oxidation states of W. These films seem to portray a condition where the valence of tungsten could show several values between W^{6+} and W^0, probably including the W^{5+} and W^{4+} states. Lines d, e and f in Fig. 4, samples prepared at 50, 75 and 100 mTorr, correspond to the most oxidized state, W^{6+} except that line d also seems to include a small amount of W^{5+} state [12], which could be causing a small shoulder in the lower energy side of the W $4f_{7/2}$ peak at about 35–36 eV and a less defined valley between the doublet. The W^{5+} state might be great importance to understand the coloration process of WO_3 and several theories has been developed around it [14,15]. Line f appears with lower resolution because of charging induced by the XPS measurement on this low-conductance sample.

To reveal the development of chemical states as a function of T_S, in Fig. 5 are showed the W 4f high-resolution energy window for films prepared at a fixed pressure of $P_O = 75$ mTorr and as a function of temperature for T_S values of RT, 250 and 500 °C. There is a decrease in the definition of the valley between the W $4f_{7/2}$ and W $4f_{5/2}$ transitions as a function of T_S, indicating that for higher T_S, the W^{6+} and W^{5+} states seem to coexist and that the substrate temperature induces chemical disorder (intermingling of W^{6+} and W^{5+} states) for the WO_3 films. Previous works, by means of XPS, found results similar to ours [12,13]. This situation allows us to conclude that the films prepared by PLD are chemically equivalent to the films prepared by other means. Thereafter, correlations exist between the chemical and the coloration state, see Table 1. The optical transparent films are prepared with predominance of W^{6+} and a certain degree of chemical disorder is present in the colored films, according to the W 4f doublet definition.

3.4. EELS analysis

The low-loss structure was obtained by means of EELS as a function of deposition parameters. In Fig. 6, the EELS spectra for films grown at RT on glass substrates, $P_O = 0$, 5, 25, 50, 75 and 100 mTorr, are presented. There are several changes in the EELS

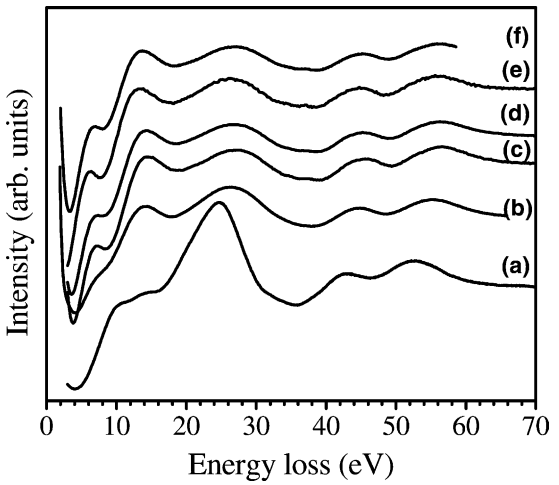

Fig. 6. EELS spectra for samples: (a) P_0T_{RT}, (b) P_5T_{RT}, (c) $P_{25}T_{RT}$, (d) $P_{50}T_{RT}$, (e) $P_{75}T_{RT}$ and (f) $P_{100}T_{RT}$. For clarity, curves have been offset vertically.

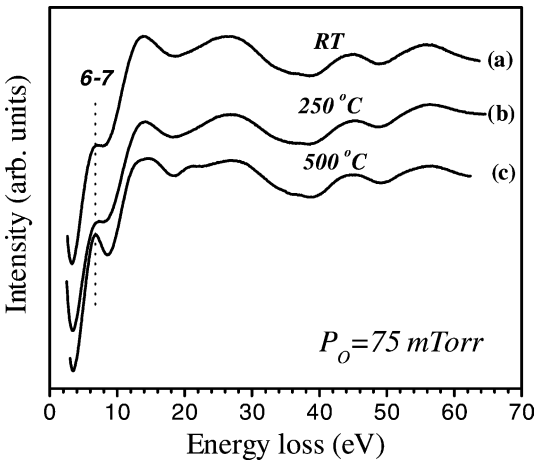

Fig. 7. EELS spectra for films grown at $P_O = 75$ mTorr. (a) $T_S =$ RT (light blue), (b) $T_S = 250$ °C (light blue), and (c) $T_S = 500$ °C (blue). For clarity, curves have been offset vertically. Note the change in the loss at 6–7 eV.

characteristics as a function of P_O and are listed in Table 2. (a) The energy-loss structure is clearly different for the P_0T_{RT} film with respect to the oxygen deposited films, (b) the main peak, measured at 24.6 eV for the P_0T_{RT} film, shifts to a higher energy, up to 27.4 eV for $P_{25}T_{RT}$ and then declines in intensity, (c) the shoulders at the low-energy-side of the main peak, around 10–15 eV in sample P_0T_{RT}, increase in intensity, becoming an intense peak for the oxidized films, at 13.4–14.6 eV and (d) an energy loss at 6.4–7.6 eV develops for tungsten oxide films and probably is a small peak at 10.2 eV for the metallic film. The peaks at the high energy side, about 43–57 eV, are interpreted as transitions from W $5p_{1/2}$ and W 5s states to unoccupied states [16].

The maximum in the energy-loss function corresponds to the energy of the bulk plasmon and is directly related to the electronic density, Eq. (2) and to the mass density, Eq. (3). The bulk-plasmon accounts for all the valence-band electrons and changes in the electronic density (number of electrons per volume unit) will cause a shift in its energy [17].

Table 2
Energy of some relevant maxima of the EELS spectra presented in Fig. 6 for the series of samples prepared at room temperature and varying the oxygen pressure

Samples	E_1 (eV)	E_2 (eV)	E_3 (eV)	E_4 (eV)	E_5 (eV)
P_0T_{RT}	10.2	14.4	24.6	43.1	52.7
P_5T_{RT}	7.6	14.3	26.4	44.8	55.3
$P_{25}T_{RT}$	7.6	14.6	27.4	45.8	56.6
$P_{50}T_{RT}$	7.4	14.4	26.8	45.4	56.4
$P_{75}T_{RT}$	6.4	13.4	26.4	45.2	56.4
$P_{100}T_{RT}$	7	13.8	26.6	45.4	56.2

It is recognized that the optical properties can be revealed by EELS and this case is not the exception, see Fig. 7. In this graph, the key parameter varied is the substrate temperature and the oxygen pressure remains constant at 75 mTorr. The three films show almost the same energy-loss structure, except for the distinction in strength of the loss at 6–7 eV, being more prominent for the films with deep-coloration ($T_S = 500$ °C). A similar effect was observed in films produced at lower and higher oxygen pressures ($P_O = 50$ and 100 mTorr). The origin of that loss has not being determined yet, although we would expect, considering its sharpness, that it could be an interband transition instead of a plasmon, as it was suggested by Hashimoto and Matsuoka [18].

The evaluation of Eqs. (2) and (3) for the series of films deposited on glass substrates is shown in Fig. 8 for the dependence of the electronic (open circles, right axis) and mass (open squares, left axis) densities as a function of depositing pressure. Straight lines were depicted to guide the eye. The error bars were calculated assuming a tolerance of ±0.2 eV in peak positioning, from the data step. There is a decrease in

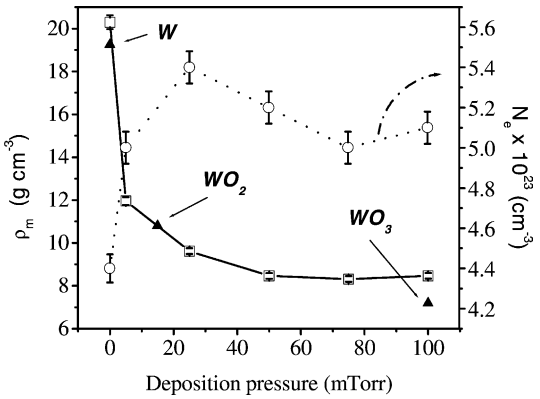

Fig. 8. Electronic (open circles) and mass (open squares) densities determined by the free-electron model using the bulk-plasmon peak positions measured by EELS.

mass density as a function of deposition pressure (or oxygen content), which can be compared with the densities of W, WO_2 and WO_3 by using the results shown in Fig. 2 of atomic concentration versus deposition pressure. Considering the relative atomic concentrations of W and O in W, WO_2 and WO_3, the corresponding oxygen pressures to obtain each one are about 0, 20 and 50 or more mTorr. These pressure values in Fig. 8 would correspond to mass densities of about 20, 10 and 8 g cm^{-3}, respectively. This is in reasonable good agreement with the theoretical mass densities for W (19.25 g cm^{-3}), WO_2 (10.8 g cm^{-3}) and WO_3 (7.2 g cm^{-3}). This indicates that the densities of the films prepared by PLD are close to the crystalline counterparts. This could be a problem since the reversibility of switching between the two chromogenic states appears to depend on the material ability to accept intercalates. Another interesting result, given in the same figure, is the electronic density. It can be seen that it presents a maximum for the film prepared at $P_O = 25$ mTorr of 5.4×10^{23} cm^{-3}. Afterwards, the electronic density declines, reaching a value of 5.1×10^{23} cm^{-3} for WO_3. This result means that the films with deep-coloration have more free-electrons per atom than the transparent films. The excess electrons must enter the t_{2g} band and the material, in principle, transforms from the transparent to the absorbing state as the electrons will have to go to delocalized states [19]. This result is of relevance in the model of intervalence charge transfer [20].

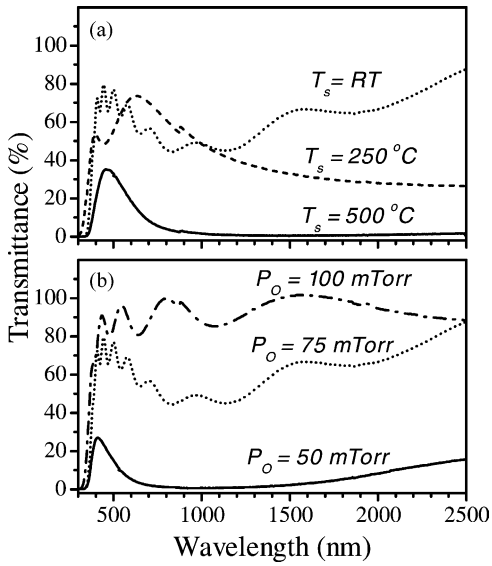

Fig. 9. Optical transmission spectra of WO_3 thin films deposited at: (a) $P_O = 75$ mTorr with variation of substrate temperature (samples: $P_{75}T_{RT}$, $P_{75}T_{250}$, $P_{75}T_{500}$) and (b) T_S = RT with variation of oxygen pressure samples: $P_{50}T_{RT}$, $P_{75}T_{RT}$, $P_{100}T_{RT}$).

3.5. Optical transmittance

Fig. 9 shows the optical transmittance spectra of thin films deposited at several deposition conditions. The effect of substrate temperature is evident in Fig. 9(a), where can be seen the diminishing of transmittance in the infrared region as T_S is incremented. The effect of the oxygen deposition pressure can be seen in Fig. 9(b), where the transmittance increases as P_O increase. Essentially, the main difference takes place in the infrared region, where a sharp decrease of transmittance is observed either for higher deposition temperatures, Fig. 9(a), or lower deposition pressures, Fig. 9(b). The film changes from a non-absorbing material (dielectric), where interference fringes can be obtained as oscillations of T versus wavelength, towards an absorbing material, metal-like where there is an achromatic response along the spectra, except in the ultraviolet region.

3.6. Post-annealing treatment

We induced thermochromic coloration cycles for some samples. To bleach annealing in air for 4 h at 300 °C, and for coloring annealing in vacuum at

500 °C during 24 h By XPS, it was found that the stoichiometric changes as a function of the annealing treatment are very small, below the instrumental resolution, i.e. fall within ±3 at.%. These results are somewhat contrary to the data presented by Durrani et al. [3] who report changes in the composition ratio by XPS measurements. Note however that Durrani et al. also report significant losses in mass and increments in films density. In divergence, the films produced by PLD remain dense with the same density, as was confirmed by EELS. This could mean that the films processed by the methodology of Durrani et al. (thermal evaporation) are less stable and susceptible to evaporation when compared to films processed by PLD. Even though the composition remains essentially unaltered by the post-thermal treatment, there are small changes in the chemical states. There is an increase in the doublet definition between W $4f_{7/2}$ and W $4f_{5/2}$ transitions for the transparent state, and, for the colored state, the W^{6+} and W^{5+} states coexist. This situation seems to indicate the post-deposition treatment to be equivalent, to some extent, to changes in deposition conditions by PLD.

The most important change measured by the electron spectroscopies as a function of the post-annealing treatment was obtained by EELS. As we mentioned above, the coloration state is manifested in this spectroscopy [18]. In Fig. 10, we can see an EELS bleaching–coloring cycle for the $P_{75}T_{500}$ sample. The strength of the loss at 6–7 eV can be noted to be more intense in the colored states in this figure. One of the proposed models to explain the coloration of WO_3 indicates that it results from interband transitions between subbands in the conduction band [18]; from the bottom of the conduction band to the top. Therefore, it is highly probable the loss at 6–7 eV to be a sign of that particular intervalence transition. As of the intervalence transition model, the bottom of the conduction band should be occupied for colored films and unoccupied for transparent films. This is in agreement with our results, since they show that the colored films have greater electron densities than the transparent films, i.e. the electronic excess should fill the bottom of the conduction band (t_{2g} band).

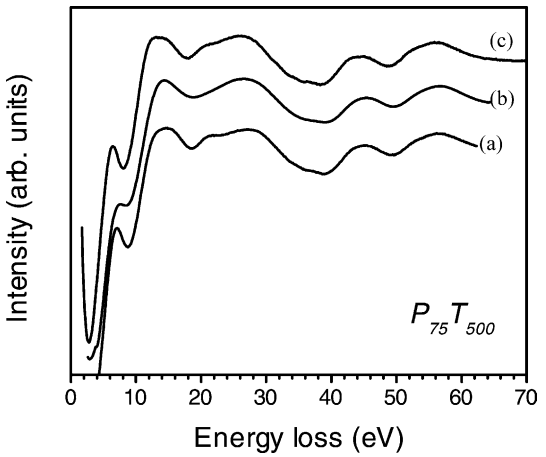

Fig. 10. EELS spectra for films grown at $P_O = 75$ mTorr and $T_S = 500$ °C. (a) Subsequent to deposition (blue), (b) after annealing in air (transparent) and (c) after annealing in vacuum (blue colored). For clarity, curves have been offset vertically. Note the change in the loss at 6–7 eV.

4. Conclusions

From the set of tungsten oxide thin films prepared by reactive PLD, varying the oxygen pressure and substrate temperature, and their characterization by XPS, AES, EELS and optical transmittance spectroscopy, the following conclusions can be obtained. The composition, chemical states, and the electronic and mass densities are strongly dependent of the substrate temperature and deposition pressure. Unlike other works, no significant modifications in the oxygen content between the colored and bleached states were observed. In consistency with the literature, it was found that the colored state is linked to the degree of chemical disorder in the samples, as was evidenced by the shape of the W 4f peaks measured by XPS. Additionally, the strength of a characteristic loss at 6–7 eV, measured by EELS, appears to be responsible of the coloration state, supporting the interband transition model [18]. Reactive PLD seems to produce films with densities close to the crystalline counterparts. This could limit the application of PLD, in this particular case, since high-density films can constraint the ion-intercalation ability of WO_3.

References

[1] P.M.S. Monk, R.J. Mortimer, D.R. Rosseinsky, Electrochromism Fundamentals and Applications, VCH, New York, 1995.

[2] C.G. Grandqvist, Handbook of Inorganic Electrochromics Materials, Elsevier, Amsterdam, 1995.
[3] S.M.A. Durrani, E.E. Khawaja, M.A. Salim, M.F. Al-Kuhaili, A.M. Al-Shukri, Sol. Energy Mater. Sol. Cells 71 (2002) 313–325.
[4] K. Bange, Sol. Energy Mater. Sol. Cells 58 (1999) 1.
[5] G. Soto, J.A. Díaz, R. Machorro, A. Reyes-Serrato, W. de la Cruz, Matt. Lett. 52 (2002) 29.
[6] J.H. Scofield, J. Electron Spectrosc. Relat. Phenom. 8 (1976) 129.
[7] C.J. Powell, A. Jablonski, I.S. Tilinin, S. Tanuma, D.R. Penn, J. Electron Spectrosc. Relat. Phenom. 98–99 (1999) 1.
[8] M. Repoux, E. Darque-Ceretti, M. Casamassima, J.P. Contour, Surf. Interface Anal. 16 (1990) 209.
[9] L.E. Davis, N.C. MacDonald, P.W. Palmberg, G.E. Riach, R.E. Weber, Handbook of Auger Electron Spectroscopy, Perkin-Elmer, Eden Praire, MN, 1978.
[10] Y.G. Shen, Y.W. Mai, Mater. Sci. Eng. A 284 (2000) 176–183.
[11] J.F. Moulder, W.F. Stickle, P.E. Sobol, K.D. Bomben, in: J. Chastain (Ed.), Handbook of X-ray Photoelectron Spectroscopy, Perkin-Elmer, Eden Praire, MN, 1992.
[12] A. Temmink, O. Anderson, K. Bange, H. Hantsche, X. Yu, Thin Solid Films 192 (1990) 211.
[13] A. Temmink, O. Anderson, K. Bange, H. Hantsche, X. Yu, Vacuum 41 (1990) 1144.
[14] V. Wittwer, O.F. Schirmer, P. Schlotter, Solid State Commun. 25 (1978) 977.
[15] O.F. Schirmer, V. Wittwer, G. Baur, G. Brandt, J. Electrochem. Soc. 124 (1977) 749.
[16] R.F. Egerton, Electron Energy Loss Spectroscopy in Electron Microscope, second ed., Plenum Press, New York, 1996; Y.G. Shen, Y.W. Mai, Mater. Sci. Eng. A 284 (2000) 176–183.
[17] C. Kittel, Introduction to Solid State Physics, sixth ed., Wiley, New York, 1986.
[18] S. Hashimoto, H. Matsuoka, J. Appl. Phys. 69 (1991) 933.
[19] C.G. Granqvist, Appl. Phys. A 57 (1993) 3.
[20] R.S. Crandall, B.W. Faughnan, Appl. Phys. Lett. 28 (1976) 95.